Journal of Power Sources 254 (2014) 137–147

Contents lists available at ScienceDirect

Journal of Power Sources

journal homepage: www.elsevier.com/locate/jpowsour

Functionalized ionic liquids based on quaternary ammonium cations with two ether groups as new electrolytes for Li/$LiFePO_4$ secondary battery

Yide Jin [a], Jianhao Zhang [a], Jianzhi Song [a], Zhengxi Zhang [a], Shaohua Fang [a,*], Li Yang [a,b,*], Shin-ichi Hirano [b]

[a] School of Chemistry and Chemical Technology, Shanghai Jiaotong University, Shanghai 200240, China
[b] Hirano Institute for Materials Innovation, Shanghai Jiaotong University, Shanghai 200240, China

HIGHLIGHTS

- New functionalized quaternary ammonium ILs with two ether groups are reported.
- They have low viscosity and good electrochemical stability.
- Li/$LiFePO_4$ cells using these IL electrolytes have good electrochemical performance.

ARTICLE INFO

Article history:
Received 13 July 2013
Received in revised form
10 December 2013
Accepted 10 December 2013
Available online 18 December 2013

Keywords:
Ionic liquids
Electrolyte
Lithium battery
Functionalized cation

ABSTRACT

New functionalized ILs based on quaternary ammonium cations with two ether groups and bis(trifluoromethanesulfonyl)imide ($TFSA^-$) anion are synthesized and characterized. Physical and electrochemical properties, including melting point, thermal stability, viscosity, conductivity and electrochemical stability are investigated for these ILs. All these ILs are liquids at room temperature except *N*,*N*-diethyl-*N*,*N*-bis(2-ethoxyethyl)ammonium TFSA (N22(2o2)(2o2)-TFSA, $T_m = 29.7$ °C), and the viscosities of *N*-methyl-*N*-ethyl-*N*-(2-methoxyethyl)-*N*-(2-ethoxyethyl)ammonium TFSA (N12(2o1)(2o2)-TFSA) and *N*-methyl-*N*-ethyl-*N*,*N*-bis(2-ethoxyethyl)ammonium TFSA (N12(2o2)(2o2)-TFSA) are 68.0 cP and 63.0 cP at 25 °C, respectively. *N*-Methyl-*N*,*N*-diethyl-*N*-(2-methoxyethyl)ammonium TFSA (DEME–TFSA) and five ILs with lower viscosity are chosen to dissolve 0.6 mol kg^{-1} of LiTFSA as IL electrolytes without additive for lithium battery. Lithium plating and striping on Ni electrode can be observed in these IL electrolytes, and cycle performances of lithium symmetrical cells are also investigated for these IL electrolytes. Li/$LiFePO_4$ cells using these IL electrolytes without additives have good cycle property at the current rate of 0.1 C, and the *N*-methyl-*N*-ethyl-*N*,*N*-bis(2-methoxyethyl)ammonium TFSA (N12(2o1)(2o1)-TFSA) and N12(2o2)(2o2)-TFSA electrolytes own better rate property than DEME–TFSA electrolyte.

1. Introduction

Ionic liquids (ILs) are molten salts with melting points at or below ambient temperature, which are consisted of various cations and anions. During the past decade, ILs have become increasingly popular in academia and industry due to their unique properties, including low vapor pressure, non-flammability, good thermal stability, great chemical and electrochemical stability and high ionic conductivity [1–3]. Their unique properties favor applications in diverse fields, such as synthesis, catalysis, separation technology, analytical chemistry, nanotechnology and electrochemistry [4–9]. For electrochemistry aspect, ILs are frequently used as potential electrolytes for different electrochemical devices, like lithium secondary battery [10–15], electrochemical double-layer capacitor [16–18], fuel cell [19,20], and dye-sensitized solar cell [21–23].

Among various kinds of ILs, quaternary ammonium ILs have been investigated widely for lithium secondary battery, because of better electrochemical stability, low cost and easy preparation

* Corresponding authors. School of Chemistry and Chemical Technology, Shanghai Jiaotong University, Shanghai 200240, China. Tel.: +86 21 54748917; fax: +86 21 54741297.
E-mail addresses: housefang@sjtu.edu.cn (S. Fang), liyangce@sjtu.edu.cn (L. Yang).

0378-7753/$ – see front matter © 2014 Elsevier B.V. All rights reserved.
http://dx.doi.org/10.1016/j.jpowsour.2013.12.048

[24–37]. Initially, some quaternary ammonium ILs without functional group are selected as electrolytes in lithium battery. Li/$LiCoO_2$ battery employing trimethylpropylammonium bis(trifluoromethanesulfonyl)imide (N1113-TFSA) electrolyte shows non-ideal cycle performance and discharge capacity decreases rapidly, despite N1113-TFSA owning good electrochemical stability [38]. Tetraethylammonium 2,2,2-trifluoro-*N*-(trifluoromethylsulfonyl) acetamide (N2222-TSAC) electrolyte also has been applied in Li/$LiCoO_2$ battery. Comparing to TFSA anion, the TSAC anion can help to lower both melting point and viscosity of IL, however, electrochemical stability decreases obviously than IL with TFSA anion, and the battery performance is also not satisfactory [39]. Furthermore, although Li/$LiCoO_2$ battery using tetraamylammonium TFSA (N5555-TFSA) electrolyte shows good cycle stability, the rate performance is limited due to the high viscosity of N5555-TFSA (554 cP at 25 °C) [39].

Ether-functionalized ILs provide more choices for applications as electrolytes in lithium battery, because incorporating short ether group with electron-donating ability into IL cation can help to reduce viscosity and melting point, and not cause the obvious degradation of electrochemical stability [40,41]. For quaternary ammonium ILs with one ether group, the most well-known IL is *N*,*N*-diethyl-*N*-methyl-*N*-(2-methoxyethyl)ammonium TFSA (DEME–TFSA). Seki et al. demonstrate excellent potential of DEME–TFSA electrolyte without any additive in Li/$LiCoO_2$ battery, the characteristics of interface of $LiCoO_2$ cathode and lithium metal anode is investigated in detail, and charge/discharge capacity retention up to 80% over 100 cycles is reported [29,42]. Besides the Li/$LiCoO_2$ battery, Tsunashima et al. have applied DEME–TFSA electrolyte in Li/$LiNi_{0.8}Co_{0.1}Mn_{0.1}O_2$ battery, achieving good cycle performance at low current rate [43]. Moreover, Sato et al. use DEME–TFSA electrolyte containing 10% vinylene carbonate (VC) in graphite/$LiCoO_2$ battery, which also shows battery performance [44]. So far, like *N*-butyl-*N*-methylpyrrolidinium TFSA (PY14-TFSA) and *N*-propyl-*N*-methylpiperidinium TFSA (PP13-TFSA) based electrolytes [45–49], the DEME–TFSA based electrolytes can be considered as good benchmark for IL electrolytes applied in lithium battery, yet the DEME–TFSA owned lower viscosity and higher conductivity than the former two ILs.

Nowadays, researchers have paid attention to ILs with two or more ether groups. For quaternary ammonium ILs, 6 quaternary ammonium ILs with two identical 2-ethoxyethyl or 4-methoxybenzyl groups have been reported firstly, and thermal properties of these ILs have been investigated [50]. 8 quaternary ammonium ILs with two, three and four identical 2-methoxyethyl groups are prepared, and their physicochemical properties are studied [51]. Recently, our group has also synthesized 11 quaternary ammonium ILs with three or four different ether groups (2-methoxyethyl or 2-ethoxyethyl) [52]. It is found that these quaternary ammonium ILs with three or four ether groups show high viscosity and low conductivity, which go against the rate performance of lithium battery, owing to big size of quaternary ammonium cation with three or four ether groups could strengthen Van der Waals interactions between cations and anions and counteract more electron-donating action of ether groups. So quaternary ammonium ILs with two ether groups might be more appropriate as electrolytes for lithium battery.

In order to find more ILs with low viscosity and good electrochemical stability for applications in lithium battery as electrolytes, we have synthesized 12 diether-functionalized quaternary ammonium ILs with 2-methoxyethyl or 2-ethoxyethyl group, their structures and abbreviations are shown in Scheme 1, except *N*,*N*-diethyl-*N*,*N*-bis(2-methoxyethyl)ammonium TFSA (N22(2o1)(2o1)-TFSA), the other 11 ILs were reported for the first time. We investigated melting point, thermal stability, viscosity, conductivity and electrochemical window of these ILs. Five ILs with lower viscosity were applied in lithium battery as new electrolytes comparing with DEME–TFSA electrolyte. Behavior of lithium redox on Ni electrode and cycle performances of lithium symmetrical cells was studied for these IL electrolytes with 0.6 mol kg^{-1} LiTFSA, and charge–discharge characteristics of Li/$LiFePO_4$ cells were examined. We found that the Li/$LiFePO_4$ cells had good cycle performances at 0.1 C rate, and cells using *N*-methyl-*N*-ethyl-*N*,*N*-bis(2-methoxyethyl)ammonium TFSA (N12(2o1)(2o1)-TFSA) and *N*-methyl-*N*-ethyl-*N*-2-methoxyethyl-*N*-2-ethoxyethylammonium TFSA (N12(2o2)(2o2)-TFSA) electrolytes showed better rate performances than DEME–TFSA electrolyte.

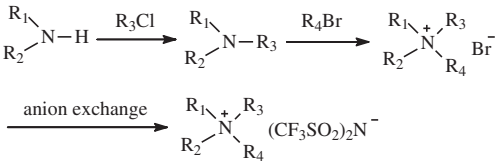

Scheme 1. Synthesis routine and structures of quaternary ammonium ILs with two ether groups.

2. Experimental

2.1. Preparation of ILs based on quaternary ammonium cations with two ether groups and bis(trifluoromethanesulfonyl)imide anion

Commercially available reagents were purchased from Sinopharm Chemical Reagent Corporation Ltd., or Alfa Aesar. Lithium bis(trifluoromethylsulfonyl) imide (LiTFSA) was kindly provided by Morita Chemical Industries Corporation Ltd. And these reagents were of analytical grade and used in this work as received.

N,*N*-Dialkylamines was reacted with chloroethyl methyl ether or chloroethyl ethyl ether at 120 °C for 48 h in a 100 mL autoclave to prepare tertiary amines with one ether group as a reference method [44]. A mixture of tertiary amine with one ether group (100 mmol), bromoethyl methyl ether or 2-bromoethyl ethyl ether (95 mmol), and methanol (20 mL) in a 250 mL flask was refluxed at 80 °C for more than 72 h under an N_2 atmosphere. The produced bromide was acquired after washing with ether. It was dissolved in acetone, and then purified with activated carbon. After filtration, the collected solution was evaporated under reduced pressure to remove the solvent. After drying in vacuum at 60 °C, the bromide and LiTFSA was dissolved in deionized water and mixed for 24 h at ambient temperature. The crude IL was dissolved with dichloromethane, and washed with deionized water until no residual halide anions in deionized water used to rinse the IL was detected with use of $AgNO_3$. The dichloromethane was removed by rotating evaporation. All the products were dried under high vacuum for more than 24 h at 110 °C. Structures of tertiary amine containing one ether group were confirmed by ^{1}H NMR (Avance III 400), and the structures of synthesized ILs were confirmed by ^{1}H NMR and ^{13}C NMR (Avance III 400), and chloroform-*d* was used as solvent for all the products. The characterization data are as follows:

N,*N*-Diethyl-*N*,*N*-di-(2-methoxyethyl)ammonium bis(trifluoromethanesulfonyl)imide (N22(2o1)(2o1)-TFSA), yield: 80%; ^{1}H NMR: δ (ppm) 3.67–3.66 (t, 4H), 3.46–3.43 (t, 4H), 3.40–3.35 (m, 4H), 3.28 (s, 6H), 1.26–1.23 (t, 6H); ^{13}C NMR: δ (ppm) 124.86–115.25, 66.79, 59.10, 58.28, 55.50, 7.57. *N*,*N*-Diethyl-*N*-2-methoxyethyl-*N*-2-ethoxyethylammonium bis(trifluoromethanesulfonyl)imide (N22(2o1)(2o2)-TFSA), yield: 75%; ^{1}H NMR: δ (ppm) 3.70–3.64 (m, 4H), 3.45–3.41 (m, 6H), 3.40–3.34 (m, 4H), 3.27 (s, 6H), 1.25–1.21 (t, 6H), 1.11–1.08 (t, 3H); ^{13}C NMR: δ (ppm) 124.81–115.33, 67.07, 65.78, 63.66, 59.12, 58.32, 58.23, 55.45, 14.83, 7.66. *N*,*N*-Diethyl-*N*,*N*-di-(2-

ethoxyethyl)ammonium bis(trifluoromethanesulfonyl)imide (N22(2o2)(2o2)-TFSA), yield: 70%; ^{1}H NMR: δ (ppm) 3.80–3.76 (m, 4H), 3.55–3.44 (m, 12H), 1.36–1.32 (t, 6H), 1.20–1.16 (t, 6H); ^{13}C NMR: δ (ppm) 124.78–115.20, 69.94, 63.60, 58.21, 55.34, 14.73, 7.54. *N*-Methyl-*N*-ethyl-*N*,*N*-di-(2-methoxyethyl)ammonium bis(trifluoromethanesulfonyl)imide (N12(2o1)(2o1)-TFSA), yield: 85%; ^{1}H NMR: δ (ppm) 3.78–3.74 (m, 4H), 3.62–3.49 (m, 6H), 3.35 (s, 6H), 3.10 (s, 3H), 1.39–1.34 (t, 3H); ^{13}C NMR: δ (ppm) 124.70–115.14, 66.78, 61.69, 59.71, 58.74, 49.07, 7.88. *N*-Methyl-*N*-ethyl-*N*-2-methoxyethyl-*N*-2-ethoxyethylammonium bis(trifluoromethanesulfonyl)imide (N12(2o1)(2o2)-TFSA), yield: 75%; ^{1}H NMR: δ (ppm) 3.82–3.75 (m, 4H), 3.63–3.48 (m, 8H), 3.36 (s, 3H), 3.11 (s, 6H), 1.40–1.35 (t, 3H), 1.20–1.16 (t, 3H); ^{13}C NMR: δ (ppm) 124.68–115.15, 66.71, 65.70, 61.61, 63.62, 59.58, 58.83, 58.46, 49.09, 14.43, 7.75. *N*-Methyl-*N*-ethyl-*N*,*N*-di-(2-ethoxyethyl)ammonium bis(trifluoromethanesulfonyl)imide (N12(2o2)(2o2)-TFSA), yield: 70%; ^{1}H NMR: δ (ppm) 3.84–3.79 (m, 4H), 3.63–3.49 (m, 10H), 3.12 (s, 3H), 1.40–1.36 (t, 3H), 1.20–1.17 (t, 3H); ^{13}C NMR: δ (ppm) 124.72–115.14, 66.81, 63.70, 61.74, 59.70, 49.17, 14.62, 7.89. *N*-Methyl-*N*-propyl-*N*,*N*-di-(2-methoxyethyl)ammonium bis(trifluoromethanesulfonyl)imide (N13(2o1)(2o1)-TFSA), yield: 85%; ^{1}H NMR: δ (ppm) 3.75–3.71 (m, 4H), 3.60–3.50 (m, 4H), 3.33 (s, 6H), 3.31–3.27 (m, 2H), 3.07 (s, 3H), 1.78–1.68 (m, 2H), 0.97–0.93 (t, 3H); ^{13}C NMR: δ (ppm) 124.74–115.18, 66.03, 65.91, 62.36, 59.21, 49.79, 16.15, 10.48. *N*-Methyl-*N*-propyl-*N*-2-methoxyethyl-*N*-2-ethoxyethylammonium bis(trifluoromethanesulfonyl)imide (N13(2o1)(2o2)-TFSA), yield: 75%; ^{1}H NMR: δ (ppm) 3.82–3.74 (m, 4H), 3.61–3.48 (m, 6H), 3.35–3.30 (m, 5H), 3.12 (s, 3H), 1.82–1.73 (m, 2H), 1.20–1.16 (t, 3H), 0.99–0.96 (t, 3H); ^{13}C NMR: δ (ppm) 124.71–115.16, 66.82, 65.80, 65.63, 63.75, 62.70, 62.08, 58.77, 49.59, 15.87, 14.87, 10.07. *N*-Methyl-*N*-propyl-*N*,*N*-di-(2-ethoxyethyl)ammonium bis(trifluoromethanesulfonyl)imide (N13(2o2)(2o2)-TFSA), yield: 70%; ^{1}H NMR: δ (ppm) 3.82–3.76 (m, 4H), 3.62–3.48 (m, 8H), 3.36–3.32 (m, 2H), 3.12 (s, 3H), 1.81–1.73 (m, 2H), 1.20–1.16 (t, 6H), 0.99–0.95 (t, 3H); ^{13}C NMR: δ (ppm) 124.68–115.09, 66.77, 65.80, 63.72, 62.09, 49.58, 15.81, 14.64, 10.00. *N*-Methyl-*N*-butyl-*N*,*N*-di-(2-methoxyethyl)ammonium bis(trifluoromethanesulfonyl)imide (N14(2o1)(2o1) -TFSI), yield: 70%; ^{1}H NMR: δ (ppm) 3.73–3.69 (t, 4H), 3.54–3.51 (m, 4H), 3.34–3.29 (m, 8H), 3.06 (s, 3H), 1.70–1.62 (m, 2H), 1.36–1.30 (m, 2H), 0.95–0.91 (t, 3H); ^{13}C NMR: δ (ppm) 124.76–115.25, 65.85, 64.40, 62.20, 59.01, 49.77, 24.31, 19.44, 13.32. *N*-Methyl-*N*-butyl-*N*-2-methoxyethyl-*N*-2-ethoxyethylammonium bis(trifluoromethanesulfonyl)imide (N14(2o1)(2o2)-TFSI), yield: 65%; ^{1}H NMR: δ (ppm) 3.75–3.72 (m, 4H), 3.57–3.44 (m, 6H), 3.35–3.31 (m, 5H), 3.07 (s, 3H), 1.71–1.63 (m, 2H), 1.37–1.28 (m, 2H), 1.16–1.12 (t, 3H), 0.95–0.91 (t, 3H); ^{13}C NMR: δ (ppm) 124.85–115.24, 67.15, 66.02, 64.51, 63.98, 62.38, 62.35, 59.12, 49.79, 24.41, 19.51, 14.92, 13.41. *N*-Methyl-*N*-butyl-*N*,*N*-di-(2-ethoxyethyl)ammonium bis(trifluoromethanesulfonyl)imide (N14(2o2)(2o2)-TFSA), yield: 70%; ^{1}H NMR: δ (ppm) 3.81–3.77 (m, 4H), 3.62–3.47 (m, 8H), 3.39–3.35 (m, 2H), 3.11 (s, 3H), 1.75–1.66 (m, 2H), 1.40–1.31 (m, 2H), 1.19–1.15 (t, 6H), 0.98–0.94 (t, 3H); ^{13}C NMR: δ (ppm) 124.74–115.13, 67.24, 64.57, 64.03, 62.45, 49.83, 24.50, 19.66, 15.04, 13.61.

2.2. Measurement

Water contents of dried ILs were detected by a moisture titrator (Metrohm 73KF coulometer) basing on Karl-Fischer method, and their values were less than 50 ppm. Density was affirmed by measuring weight of prepared IL (1.0 mL) at 25 °C.

Calorimetric measurement of each IL was performed by using a differential scanning calorimeter (DSC, Perkin–Elmer Pyris 1) in the temperature range from −60 °C to 60 °C. Each sample with an average weight of 4–6 mg was sealed in aluminum pan in a dry chamber, and then heated and cooled at scan rate of 10 °C min^{-1}. Thermal data were collected during heating in the second heating-cooling scan. Thermal stabilities were measured with TGA (Perkin–Elmer, 7 series thermal analysis system). Each sample with an average weight of 4–6 mg was placed in a platinum pan, and heated at 10 °C min^{-1} from room temperature to 600 °C under nitrogen. Viscosity of each IL was got by using viscometer (DV-III ULTRA, Brookfield Engineering Laboratories, Inc.). Ionic conductivity was measured by using DDS-309+ conductivity meter in a dry chamber. Electrochemical windows of these ILs were tested by linear sweep voltammogramms (LSV, scan rate 10 mV s^{-1}) in an argon-filled UNILAB glove box ([O_2] < 1 ppm, [H_2O] < 1 ppm). Working electrode was glassy carbon disk (3 mm diameter), and lithium metal was used as both counter and reference electrodes (surface area of 10 mm × 10 mm and thickness of 1.5 mm).

Plating and stripping behaviors of lithium in IL electrolytes (IL with 0.6 mol kg^{-1} LiTFSA) was determined by cyclic voltammogramms method (CV, scan rate 10 mV s^{-1}) in the glove box. Nickel disk (2 mm diameter) was used as working electrode and lithium metal was used as both counter and reference electrodes (surface area of 10 mm × 10 mm and thickness of 1.5 mm). The nickel electrode was polished in the usage of alumina paste (d = 0.1 μm). And the Ni electrode was washed by deionized water then dried under vacuum. The LSV and CV tests were performed by CHI660D electrochemistry workstation (CH Instruments, Inc., USA) at room temperature (25 °C).

Lithium symmetrical coin cell (CR2016 stainless steel cell, 16 mm diameter disc of lithium foil and 19 mm borosilicate glass separator (GF/A, Whatman)) was constructed in the glove box. After the cell stayed at open circuit for 36 h, charge–discharge (C–D) cycling was conducted on CT2001A cell test instrument (LAND Electronic Co., Ltd.) at room temperature using a current density of 0.1 mA cm^{-2} for 32 min (16 min "charge" and 16 min "discharge"). Impedance responses of symmetrical cell were measured before and after the cycling by using CHI660D electrochemistry workstation (100 KHz-100 mHz; applied voltage 5 mV) at room temperature.

Li/$LiFePO_4$ coin cell (CR2016 stainless steel cell) was assembled as test cell to evaluate performances of IL electrolytes for lithium secondary battery basing on the performances of lithium ion phosphate cathode. Lithium foil (battery grade) was used as a negative electrode and positive electrode was fabricated by spreading the mixture of $LiFePO_4$ (kindly provided by PULEAD Technology Industry Co., LTD, China), acetylene black and PVDF (firstly dissolved in *N*-methyl-*N*-2-pyrrolidone) with a weight ratio of 8:1:1 on aluminum current collector (battery use). Loading of active materials was about ca. 1.5–2.0 mg cm^{-2} and this thinnish electrode was used without pressing. Glass filter made of borosilicate glass (GF/A, Whatman) was used as separator. Cell was assembled in the glove box, and all the components of cell were dried under vacuum before using. Cell performances were examined by the charge–discharge (C–D) cycling tests using a CT2001A cell test instrument (LAND Electronic Co., Ltd.) at 25 °C and at different current rates (0.1 C–2.0 C), current was determined by theoretical capacity of 170 mAh g^{-1} for Li/$LiFePO_4$ cell. The cells were sealed and then stayed at room temperature for 4 h before the performance tests. Constant current charge–discharge cycles were conducted between 2.0 and 4.0 V (vs. Li/Li$^+$). Charging included two processes: (1) constant current at a rate, cut-off voltage of 4.0 V; (2) constant voltage at 4.0 V, held for 1 h. And discharging had one process: constant current at the same rate, cut-off voltage of 2.0 V.

3. Results and discussion

3.1. Properties of these ILs

Physicochemical properties of these quaternary ammonium ILs with two ether groups, including melting point, density, viscosity,

conductivity and thermal decomposition temperature, are listed in Table 1. In order to discuss properties clearly, these ILs were classified to N12 series, N22 series, N13 series and N14 series basing on the substituent groups at central nitrogen atom except the two ether groups.

Phase transitions of these ILs were investigated by differential scanning calorimetry (DSC), and DSC traces of four ILs are shown in Fig. 1 as examples. N22(2o2)(2o2)-TFSA (Fig. 1(b)) and N22(2o1)(2o2)-TFSA (Fig. 1(c)) owned a crystallization transition (T_c) before melting transition (T_m), and N22(2o1)(2o1)-TFSA (Fig. 1(d)) showed a solid–solid transition (T_{s-s}) between crystallization transition and melting transition. Like N12(2o1)(2o1)-TFSA (Fig. 1(a)), the rest eight ILs did not show any phase transition behaviors until −60 °C, which was interior temperature limit of our DSC measurement, and we denoted their melting points by "<−60 °C" like several published papers [50,53].

Usually, for imidazolium, quaternary ammonium, phosphonium, pyrrolidinium, piperidinium and guanidinium ILs, introducing one short ether group into cation has been proved to be helpful to reduce melting points of ILs, due to weakening electrostatic interaction between cation and anion (which resulted from electron donation action of ether group), reducing symmetry of cations, and high flexibility of ether group [53–57]. When two 2oR ether groups were incorporated into quaternary ammonium cations, due to stronger electron-donating effect of more ether groups, some ILs with low melting points could also be acquired. As shown in Table 1, melting points of N12 series, N13 series and N14 series ILs were all lower than −60 °C. For N22 series ILs, N22(2o1)(2o1)-TFSA, N22(2o1)(2o2)-TFSA and N22(2o2)(2o2)-TFSA owned melting points of 3.3, 1.1, and 28.9 °C respectively, which might be ascribed to higher symmetry of N22 series cations overwhelms the electron-donating effect of two ether groups.

Thermal stabilities of these ILs were examined by variable-temperature TGA experiments. Like N12 series ILs, which are shown in Fig. 2 as examples, all these quaternary ammonium ILs with two ether groups had one-stage decomposition behavior. Generally, T_d values of ILs with $TFSA^-$ anion decreased with increasing of number of ether groups in IL cations, basing on the thermal decomposition temperatures of 1,3-dialkylimidazolium, trialkylimidazolium, pyrrolidinium, piperidinium and guanidinium ILs without and with one or two ether groups [54–61]. Likewise, in terms of Table 1 and published data [52], for quaternary ammonium ILs without and with one, two, three or four ether groups, thermal stability also decreased with increasing of number of ether groups. For example, the thermal decomposition temperature decreased in following order: N1224-TFSA, 400 °C > DEME–TFSA, 390 °C > N12(2o1)(2o1)-TFSA, 354.5 °C > $N2(2o1)_3$-TFSA, 331.5 °C > $N(2o1)_4$-TFSA, 315.7 °C. Though more ether groups could cause a negative effect to thermal stability of ILs, the thermal decomposition temperatures of these quaternary ammonium ILs with two ether groups were still higher than 340 °C.

Viscosity of IL is generally affected by the ion symmetry, ion size, and ion interactions (such as electrostatic and Van der Waals attractions) [62]. The viscosity of IL is an important parameter for evaluating its use as media in chemical and electrochemical applications, and ILs with low viscosity can be beneficial for the mass transport properties. Usually, for imidazolium, quaternary ammonium, phosphonium, pyrrolidinium, piperidinium and guanidinium ILs, replacing one alkyl group in the cations by one ether group with the similar size and formula weight, could help to reduce viscosity of IL, due to weakening electrostatic interaction between the cation and anion which resulted from the electron-donating action of ether group [53–57]. When two ether groups were introduced into pyrrolidinium, guanidinium and

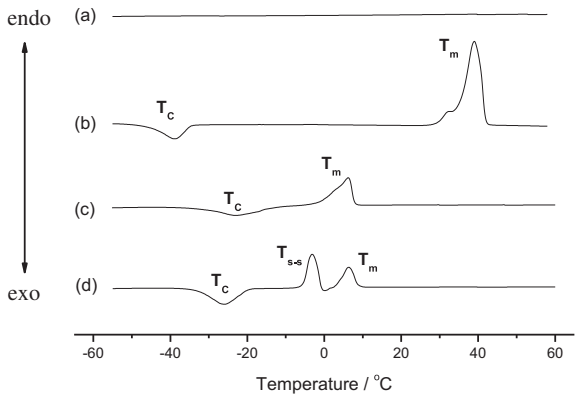

Fig. 1. DSC curves of (a) N12(2o1)(2o1)-TFSA, (b) N22(2o2)(2o2)-TFSA, (c) N22(2o1)(2o2)-TFSA, (d) N22(2o1)(2o1)-TFSA.

Table 1
Physical and thermal properties of quaternary ammonium ILs with two ether groups.

ILs	Mw[a] (g mol^{-1})	T_m[b] (°C)	d[c] (g cm^{-3})	η[d] (mPa s)	σ[e] (mS cm^{-1})	T_d[f] (°C)
N12(2o1)(2o1)-TFSA	456.4	<−60	1.34	72.1	2.06	354.5
N12(2o1)(2o2)-TFSA	470.4	<−60	1.32	68.0	1.96	354.9
N12(2o2)(2o2)-TFSA	484.4	<−60	1.28	63.0	1.88	350.6
N22(2o1)(2o1)-TFSA	470.4	3.3	1.37	79.1	1.86	351.7
N22(2o1)(2o2)-TFSA	484.4	1.1	1.32	73.8	1.84	343.9
N22(2o2)(2o2)-TFSA	498.4	28.9	–	–	–	347.8
N13(2o1)(2o1)-TFSA	470.4	<−60	1.34	86.0	1.46	354.2
N13(2o1)(2o2)-TFSA	484.4	<−60	1.31	84.2	1.44	346.5
N13(2o2)(2o2)-TFSA	498.4	<−60	1.28	80.1	1.40	347.5
N14(2o1)(2o1)-TFSA	484.4	<−60	1.35	92.0	1.13	352.4
N14(2o1)(2o2)-TFSA	498.4	<−60	1.30	91.0	1.04	342.7
N14(2o2)(2o2)-TFSA	512.4	<−60	1.28	87.9	1.12	343.4
DEME–TFSA	426.4	<−60[g]	1.42[g]	69.0[g]	2.60[g]	390.0[g]

[a] Molecular Weight.
[b] Melting point.
[c] Density at 25 °C.
[d] Viscosity at 25 °C.
[e] Conductivity at 25 °C.
[f] Decomposition temperature of 10% weight loss.
[g] Literature data [55].

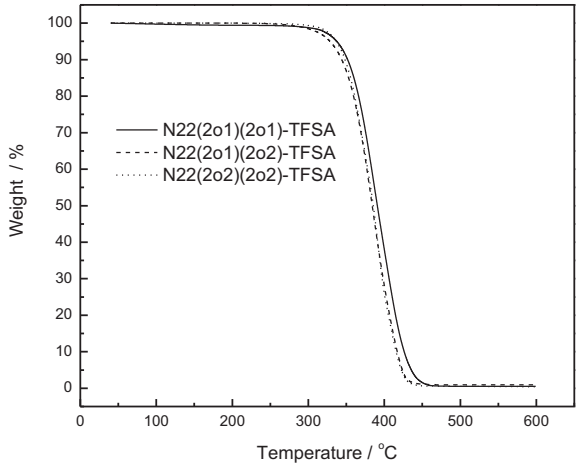

Fig. 2. TGA traces of N22(2o1)(2o1)-TFSA, N22(2o1)(2o2)-TFSA and N22(2o2)(2o2)-TFSA.

trialkylimidazolium ILs, some ILs showed viscosity close to their counterparts ILs without and with one ether group of smaller cation sizes [58–60]. According to Table 1, for these quaternary ammonium ILs with two ether groups, N12 series ILs owned viscosity close to that of DEME–TFSA (69 cP at 25 °C), and the viscosities of N12(2o1)(2o2)-TFSA (68.0 cP) and N12(2o2)(2o2)-TFSA (63.0 cP) were lower than DEME–TFSA. Moreover, though the viscosities of N22 series, N13 series and N14 series ILs were higher than DEME–TFSA, their viscosities were still all lower than 100 cP, which were obviously lower than the viscosities of quaternary ammonium ILs with three or four ether groups [52].

In terms of Table 1, for the four ILs series, their viscosities increased as follows: N12 series < N22 series < N13 series < N14 series when the two ether groups in IL cations were identical, which could be ascribed to increasing of cation sizes. But in each ILs series, if IL cation with more 2-ethoxyethyl (2o2), lower viscosity the IL would have, despite 2-ethoxyethyl group had bigger size than 2-methoxyethyl (2o1) group. Similarly, comparing the viscosities of pyrrolidinium, quaternary ammonium, 1,3-dialkylimidazolium ILs with one 2o1 group or one 2o2 group, it could be found that 2o2 group was more effective to reduce viscosity than 2o1 group [63]. This phenomenon indicated that other factors might affect the IL viscosity besides ion symmetry, ion size and ion interactions, which might be attributed to influence of ion pairs or complexes in ILs on viscosity.

Fig. 3 shows temperature dependence of viscosity for N12 series ILs which was investigated over the temperature range 25–80 °C, and η (T) behavior was fitted by a Vogel–Tammann–Fulcher (VTF) Eq. (1) using the software of Origin 7.5:

$$\eta = \eta_0 \exp\left(\frac{B}{T - T_0}\right) \quad (1)$$

where T is absolute temperature, η_0 (cP), B (K) and T_0 (K) are adjustable parameters. The η_0 is a temperature-independent prefactor, B is pseudo-activation energy and T_0 is related to ideal glass transition temperature [64,65]. The best-fit η_0 (cP), B (K) and T_0 (K) parameters for all these ILs are given in Table 2 along with corresponding fitting coefficient R^2 values. The viscosities of these ILs were very well fitted by VTF model over the temperature range studied. From Table 2, it was learned that usually if IL owned smaller T_0 value, bigger B value it would have, and IL viscosity was more sensitive with temperature changing over the temperature

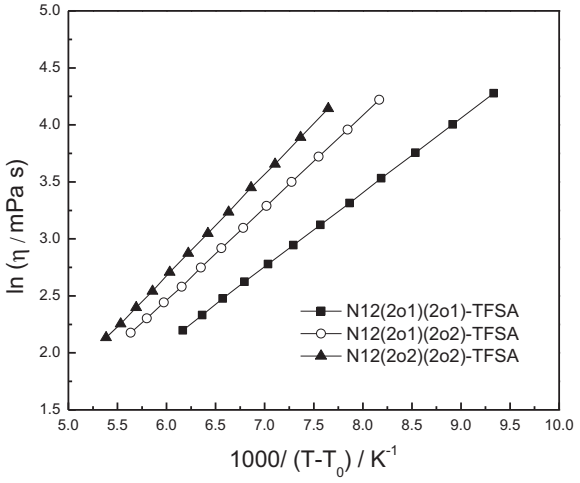

Fig. 3. VTF plots of viscosity for N12(2o1)(2o1)-TFSA, N12(2o1)(2o2)-TFSA and N12(2o2)(2o2)TFSA.

Table 2
VTF equation parameters of viscosity for quaternary ammonium ILs with two ether groups.

ILs	η_o (mPa s)	B (K)	T_o (K)	R^2
N12(2o1)(2o1)-TFSA	0.162 (±7%)	653.1 (±3%)	190.9 (±1%)	0.99999
N12(2o1)(2o2)-TFSA	0.091 (±8%)	810.9 (±2%)	175.7 (±1%)	0.99999
N12(2o2)(2o2)-TFSA	0.070 (±14%)	889.7 (±5%)	167.4 (±2%)	0.99997
N22(2o1)(2o1)-TFSA	0.163 (±9%)	670.1 (±3%)	189.8 (±1%)	0.99998
N22(2o1)(2o2)-TFSA	0.180 (±6%)	644.9 (±2%)	191.0 (±1%)	0.99999
N13(2o1)(2o1)-TFSA	0.098 (±8%)	738.2 (±3%)	189.2 (±1%)	0.99999
N13(2o1)(2o2)-TFSA	0.079 (±8%)	809.3 (±2%)	182.0 (±1%)	0.99999
N13(2o2)(2o2)-TFSA	0.083 (±10%)	814.0 (±3%)	179.6 (±1%)	0.99998
N14(2o1)(2o1)-TFSA	0.093 (±5%)	809.5 (±2%)	180.9 (±1%)	0.99999
N14(2o1)(2o2)-TFSA	0.104 (±8%)	788.4 (±3%)	181.9 (±1%)	0.99999
N14(2o2)(2o2)-TFSA	0.076 (±9%)	842.6 (±3%)	178.7 (±1%)	0.99999

The percentage standard errors for η_o, B and T_o have been included, and R^2 is the VTF fitting parameter.

studied according to Eq. (1). Among these ILs, N12(2o2)(2o2)-TFSA had minimum T_0 value and maximum B value, while N22(2o1)(2o2)-TFSA had biggest T_0 value and smallest B value. And in N12 series, N13 series and N14 series, IL with two 2-ethoxyethyl groups had smaller T_0 value and higher B value.

Substituting one alkyl group in IL cation by one ether group with the similar size and formula weight could also be beneficial to increase conductivity [53–57]. When two ether groups were introduced into cations of ILs, for pyrrolidinium, piperidinium, guanidinium and trialkylimidazolium ILs, the IL conductivity decreased comparing with the counterpart ILs based on smaller cation sizes with or without one ether group, because of the increasing of cation sizes and Van der Waals interactions between cations and anions [58–60]. Likewise, for these quaternary ammonium ILs with two ether groups, their conductivities were in the range of 1.02–2.06 mS cm^{-1} at room temperature, which were smaller than DEME–TFSA (2.6 mS cm^{-1}) [55]. And as the viscosity property, the conductivities of quaternary ammonium ILs with two ether groups were higher than the quaternary ammonium ILs with three or four ether groups. For the four ILs series, their conductivities decreased as follows: N12 series > N22 series > N13 series > N14 series when the two ether groups in ILs series were identical, due to obviously increasing of cation sizes. In each ILs series, IL conductivity decreased with increasing of cation size, if IL had more 2-methoxyethyl group, higher conductivity it would have. Considering viscosity of these quaternary ammonium ILs, it was interestingly found that IL with lowest viscosity did not show highest conductivity in each ILs series, and it is possible that IL with smaller cation size might have higher conductivity when their viscosities did not differ apparently from each other.

Temperature dependence of conductivity was also investigated for these quaternary ammonium ILs with two ether groups in temperature range of 25–80 °C, and VTF plots for N12 series ILs according to Eq. (2) are illustrated in Fig. 4 as example.

$$\sigma = \sigma_0 \exp\left(\frac{-B}{T - T_0}\right) \quad (2)$$

where T is absolute temperature, σ_0 (mS cm^{-1}), B (K) and T_0 (K) are adjustable parameters of Eq. (2). The σ_0 is maximum electrical conductivity (that it would have at infinite temperature), B is related to activation energy for electrical conduction and T_0 is ideal glass transition temperature at which the conductivity goes to zero. The best-fit σ_0, B and T_0 parameters for all these ILs are given in Table 3 along with corresponding fitting coefficient R^2 values. Like the temperature dependence of viscosity, the temperature dependence of conductivity for these ILs suited the VTF model very well over the temperature range studied. From Eq. (2), it could be

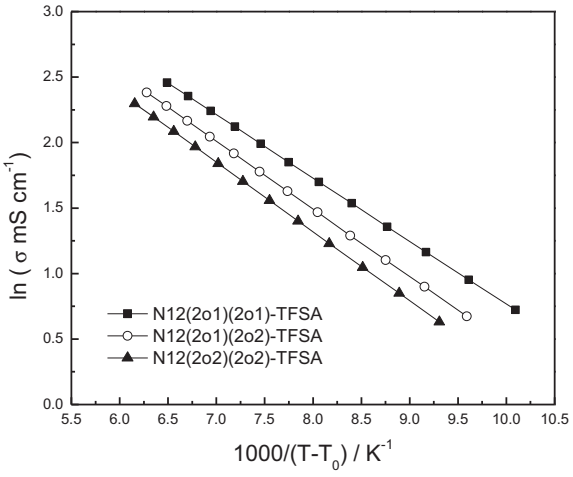

Fig. 4. VTF plots of conductivity for N12(2o1)(2o1)-TFSA, N12(2o1)(2o2)-TFSA, N12(2o2)(2o2)-TFSA.

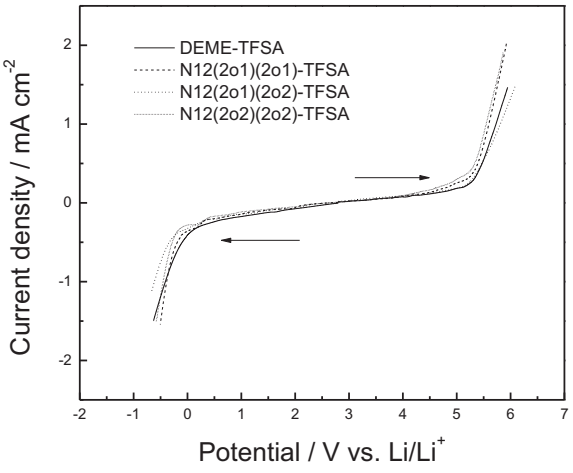

Fig. 5. Linear sweep voltammograms of DEME–TFSA, N12(2o1)(2o1)-TFSA, N12(2o1)(2o2)-TFSA and N12(2o2)(2o2)-TFSA at 25 °C. Working electrode: glassy carbon; counter and reference electrode: lithium metal; scan rate: 10 mV s^{-1}.

inferred that if IL owned bigger B value, the conductivity would be more insensitive with temperature changing over the studied temperature range. Among these ILs, N14(2o2)(2o2)-TFSA had maximum B value while N14(2o1)(2o1)-TFSA owned smallest B value. By the comparisons of T_0 value between viscosity and conductivity for the same ionic liquid, it could be found that T_0 value of viscosity was smaller than T_0 value of conductivity and B value of viscosity was bigger than that of conductivity.

The electrochemical stabilities of these ILs were investigated by linear sweep voltammogram (LSV). LSV curves of DEME–TFSA and N12 series ILs at 25 °C are shown in Fig. 5 as examples. The cathodic limiting potentials of DEME–TFSA and N12(2o1)(2o1)-TFSA were about 0.1 V and 0.2 V versus Li/Li^+, and their anodic limiting potentials were about 5.3 versus Li/Li^+. So their electrochemical windows were about 5.2 and 5.1 V, respectively. All the results of LSV measurements are listed in Table 4. As already reported, introducing one ether group into quaternary ammonium cation would reduce electrochemical stability [39]. And when two ether groups were incorporated into quaternary ammonium cation, according to Table 4, the cathodic limiting potentials of these ILs were slightly higher than that of DEME–TFSA and the anodic limiting potentials of these ILs and DEME–TFSA were almost the same, so the electrochemical windows of these quaternary ammonium ILs with two ether groups were slightly narrower than DEME–TFSA. In addition, the electrochemical window values of these ILs were obviously higher than those of quaternary ammonium ILs with three or four ether groups referring to published data [52]. Although the electrochemical stabilities of these ILs with two ether groups were not as good as the quaternary ammonium ILs without ether group [66], their electrochemical windows were still higher than 5.0 V, and these quaternary ammonium ILs with two ether groups could be regarded as ILs with good electrochemical stability.

3.2. Lithium redox in IL electrolytes

Generally, the addition of lithium salts in ILs can cause increasing of viscosity and decreasing of conductivity. Table 5 shows the viscosity and conductivity of these quaternary ammonium ILs and DEME–TFSA with 0.6 mol kg^{-1} of LiTFSA at room temperature. Referring to the viscosity and conductivity of pure ILs in Table 1, it could be found that the ILs with lower viscosity and higher conductivity also showed lower viscosity and higher conductivity for their solutions with lithium salts.

Five IL with lower viscosity (N12(2o1)(2o1)-TFSA, N12(2o1)(2o2)-TFSA, N12(2o2)(2o2)-TFSA, N22(2o1)(2o1)-TFSA and N12(2o1)(2o2)-TFSA), along with DEME–TFSA were chosen to be added with 0.6 mol kg^{-1} of LiTFSA and investigated as IL electrolytes for lithium secondary battery. Lithium redox properties

Table 3
VTF equation parameters of conductivity for quaternary ammonium ILs with two ether groups.

ILs	σ_o (mS cm^{-1})	B (K)	T_o (K)	R^2
N12(2o1)(2o1)-TFSA	269.3 (±3%)	483.2 (±2%)	199.1 (±1%)	0.99999
N12(2o1)(2o2)-TFSA	279.2 (±3%)	517.5 (±2%)	193.9 (±1%)	0.99999
N12(2o2)(2o2)-TFSA	260.5 (±3%)	530.3 (±2%)	190.7 (±1%)	0.99999
N13(2o1)(2o1)-TFSA	299.5 (±20%)	522.4 (±10%)	200.1 (±3%)	0.99974
N13(2o1)(2o2)-TFSA	259.0 (±3%)	509.6 (±1%)	200.4 (±2%)	0.99999
N13(2o2)(2o2)-TFSA	250.1 (±6%)	526.6 (±3%)	196.6 (±1%)	0.99997
N22(2o1)(2o1)-TFSA	232.5 (±4%)	457.9 (±2%)	203.5 (±1%)	0.99999
N22(2o1)(2o2)-TFSA	257.8 (±5%)	511.0 (±2%)	194.7 (±1%)	0.99999
N22(2o2)(2o2)-TFSA	240.0 (±2%)	506.1 (±1%)	195.3 (±1%)	1
N14(2o1)(2o1)-TFSA	155.0 (±2%)	443.1 (±1%)	208.1 (±1%)	0.99999
N14(2o1)(2o2)-TFSA	178.4 (±9%)	498.9 (±5%)	200.6 (±1%)	0.99994
N14(2o2)(2o2)-TFSA	302.0 (±3%)	606.5 (±2%)	289.7 (±1%)	0.99999

The percentage standard errors for σ_o, B and T_o have been included, and R^2 is the VTF fitting parameter.

Table 4
Electrochemical windows of quaternary ammonium ILs with two ether groups at 25 °C.

ILs	Cathodic limiting potential	Anodic limiting potential	Electrochemical window
	V vs. Li/Li^+	V vs. Li/Li^+	V
N12(2o1)(2o1)-TFSA	0.2	5.3	5.1
N12(2o1)(2o2)-TFSA	0.2	5.2	5.0
N12(2o2)(2o2)-TFSA	0.3	5.3	5.0
N22(2o1)(2o1)-TFSA	0.2	5.2	5.0
N22(2o1)(2o2)-TFSA	0.3	5.3	5.0
N13(2o1)(2o1)-TFSA	0.2	5.3	5.1
N13(2o1)(2o2)-TFSA	0.3	5.3	5.0
N13(2o2)(2o2)-TFSA	0.3	5.3	5.0
N14(2o1)(2o1)-TFSA	0.2	5.2	5.0
N14(2o1)(2o2)-TFSA	0.2	5.3	5.1
N14(2o2)(2o2)-TFSA	0.1	5.2	5.1
DEME–TFSA	0.1	5.3	5.2

Working electrode: glassy carbon; counter and reference electrode: lithium metal; scan rate: 10 mV s^{-1}.

Table 5
Viscosity and conductivity of these ILs with 0.6 mol kg^{-1} of LiTFSA at 25 °C.

IL electrolytes	η (mPa s)	σ (mS cm^{-1})
N12(2o1)(2o1)-TFSA	203.1	0.83
N12(2o1)(2o2)-TFSA	182.3	0.78
N12(2o2)(2o2)-TFSA	165.2	0.74
N22(2o1)(2o1)-TFSA	230.8	0.70
N22(2o1)(2o2)-TFSA	212.6	0.66
N13(2o1)(2o1)-TFSA	243.1	0.60
N13(2o1)(2o2)-TFSA	238.8	0.58
N13(2o2)(2o2)-TFSA	231.2	0.54
N14(2o1)(2o1)-TFSA	263.6	0.48
N14(2o1)(2o2)-TFSA	259.3	0.42
N14(2o2)(2o2)-TFSA	248.1	0.46
DEME–TFSA	190.9	0.96

were examined by cyclic voltammogram (CV) method at 25 °C. CV curves are shown in Fig. 6(a)–(f), and plating and stripping of lithium on Ni electrode can be clearly observed. In first cycle for DEME–TFSA electrolyte (Fig. 6(a)), deposition of lithium was at about −0.13 V vs. Li/Li$^+$, and anodic peak at about +0.41 V vs. Li/Li$^+$ in returning scan was related to dissolution of lithium. A small cathodic peak at about +0.35 V vs. Li/Li$^+$ which existed in the first cycle might be assigned to electrochemical reduction of IL electrolyte, and electrochemical reduction products could be assumed to generate a solid electrolyte interface (SEI) film on Ni electrode. Peak currents of the lithium redox decreased with cycle number, and it suggested the SEI film changed so that the lithium redox was restrained. Moreover, the currents of cathodic peak at about +0.35 V vs. Li/Li$^+$ also decreased, and it could mean that the SEI film generated in the first cycle also restrained the reduction of electrolyte.

Some differences of lithium redox behaviors on the Ni electrode were found in Fig. 6(a)–(f) for these IL electrolytes. The peak currents of lithium redox were different, and how the cathodic and anodic peaks of lithium changed with the cycle number was also different. The DEME–TFSA electrolyte showed bigger peak currents of lithium redox among these IL electrolytes. The cathodic peaks of lithium decreased more obviously with cycle number in DEME–

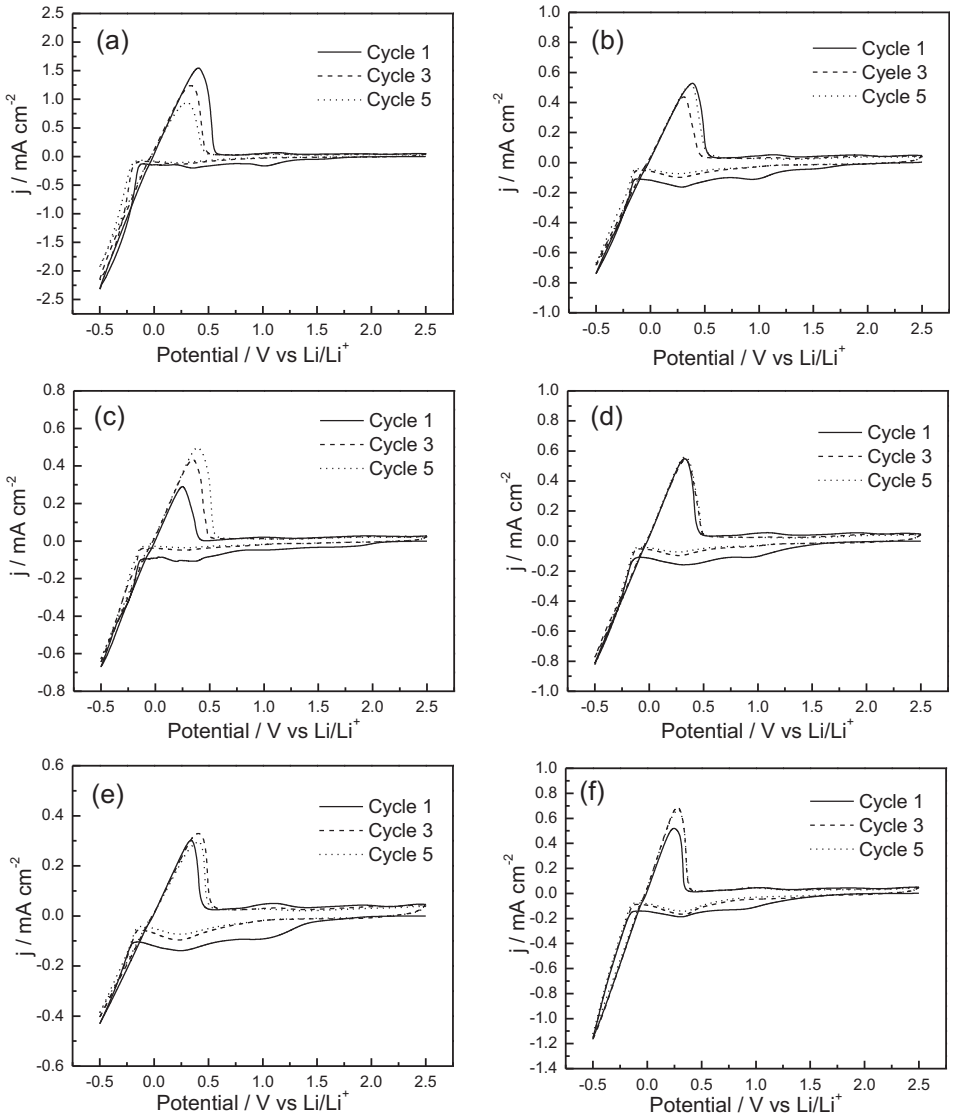

Fig. 6. Cyclic voltammograms of these IL electrolytes with 0.6 mol kg^{-1} LiTFSA at 25 °C (−0.5 V to 2.5 V versus Li/Li$^+$). (a) DEME–TFSA electrolyte, (b) N12(2o1)(2o1)-TFSA electrolyte, (c) N12(2o1)(2o2)-TFSA electrolyte, (d) N12(2o2)(2o2)-TFSA electrolyte, (e) N22(2o1)(2o1)-TFSA electrolyte and (f) N22(2o1)(2o2)-TFSA electrolyte. Working electrode, Ni; counter electrode, Li; reference electrode, Li; scan rate, 10 mV s^{-1}.

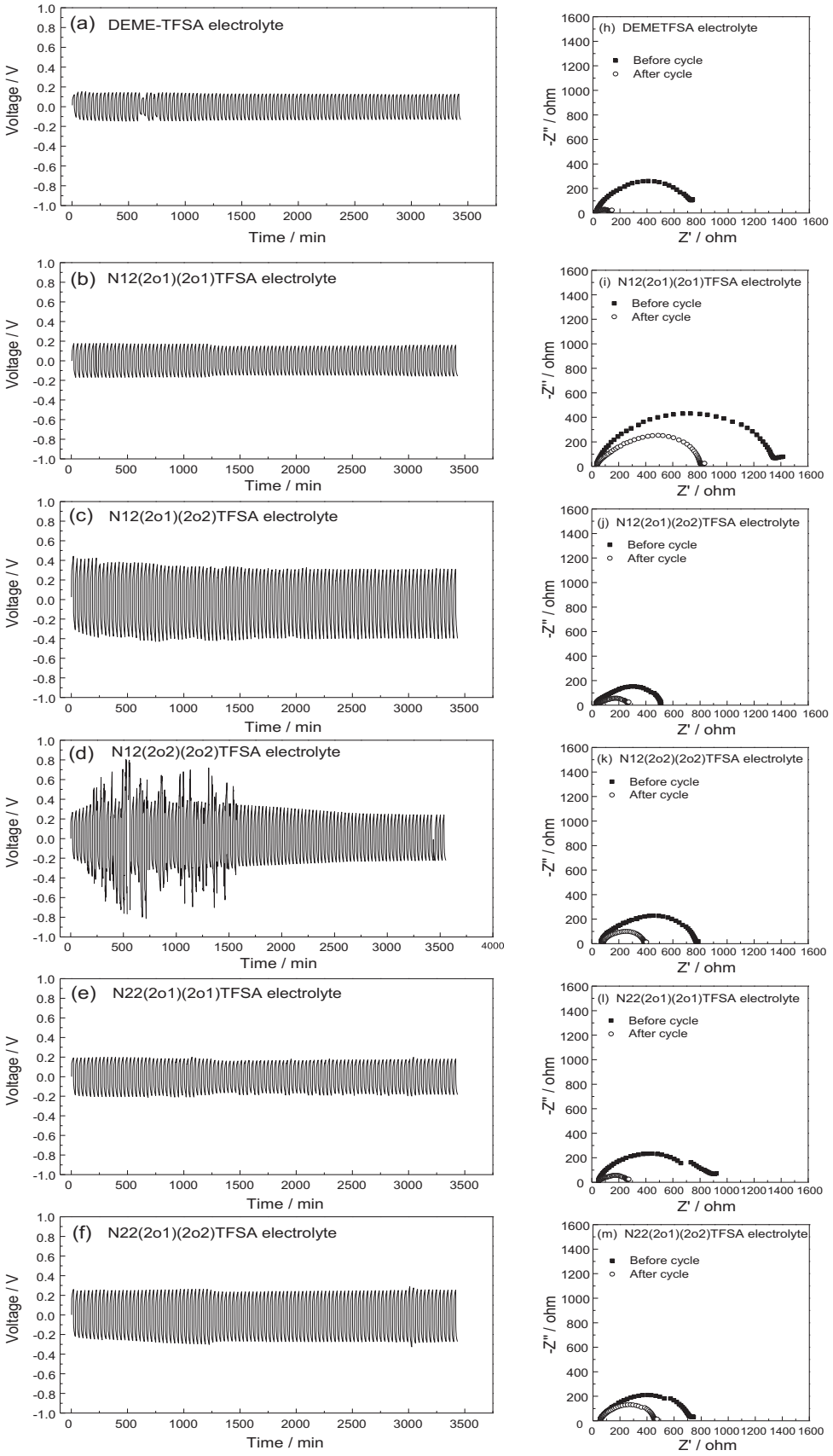

Fig. 7. Li symmetrical cell cycling and EIS results: 16 mm Li disc, 0.1 mA cm^{-2} constant current for 16 min, 100 cycles at room temperature using the IL electrolytes with 0.6 mol kg^{-1} LiTFSA; (a) and (h) DEME–TFSA electrolyte, (b) and (i) N12(2o1)(2o1)-TFSA electrolyte, (c) and (j) N12(2o1)(2o2)-TFSA electrolyte, (d) and (k) N12(2o2)(2o2)-TFSA electrolyte, (e) and (l) N22(2o1)(2o1)-TFSA electrolyte, (f) and (m) N22(2o1)(2o2)-TFSA electrolyte.

TFSA electrolyte, and the cathodic peaks of lithium almost overlapped in N22(2o1)(2o2)-TFSA electrolyte (Fig. 6(f)). The anodic peaks of lithium also decreased obviously with cycle number in DEME–TFSA electrolyte, and the anodic peaks of lithium in other five IL electrolytes did not decrease with cycle number. For instance, the anodic peaks of lithium with cycle number in N12(2o2)(2o2)-TFSA electrolyte (Fig. 6(d)) were almost overlapped. Hence, structure of cation of IL might affect the constitution of passivation film generated on Ni electrode, which would also impact the deposition and dissolution of lithium in IL electrolyte, and introducing two ether groups into quaternary ammonium cation might be beneficial to reversibility of lithium redox.

Furthermore, a cathodic peak in range of 0.8 V–1.2 V versus Li/Li^+ and one anodic peak in the range from 0.9 V to 1.2 V versus Li/Li^+ could be found in first cycle for the six IL electrolytes, which might be caused by the reactions of the trace water or oxygen in electrolyte on Ni electrode, and these peaks disappeared or peak currents decreased in subsequent cycles because of the passivation film formed in the first cycle. These kinds of cathodic and anodic peaks caused by the trace impurities, could also be found in the reported experimental results of CV for some other IL electrolytes [33,61,67,68].

3.3. Cyclic performance of IL electrolytes in lithium symmetrical cells

Cycling test for 100 cycles and electrochemical impedance spectra (EIS) of lithium symmetrical cell were used to investigate the interfacial characteristics of IL electrolyte/lithium metal [69–72]. Lithium symmetrical cell was kept at open circuit for some time before cycling test in order to generate a stable passivation layer on lithium metal [58,60,73]. Fig. 7(a)–(f) shows the results of cycling test and Fig. 7(h)–(m) shows the results of EIS before and after cycling test. The intercept with the real axis of impedance response at high frequency was assigned to electrolyte bulk resistance, and the diameter of the semicircle was related to the interfacial resistance of IL electrolyte/lithium metal [74,75].

For N12(2o2)(2o2)-TFSA electrolyte (Fig. 7(d)), the voltage profile fluctuated remarkably before the 50th cycle and then restored to stable state. This kind of behavior did not indicate short-circuiting resulted from lithium dendritic growth but that a reorganization of lithium surface into a different morphology might take place [69,70,76]. For the other five IL electrolytes, the voltage profile did not show the obvious fluctuating behavior during the 100 cycles, which implied that a stable SEI film could form on lithium metal. Among these IL electrolytes, DEME–TFSA electrolytes had lower voltage profile (about 0.15 V), and the voltage profile of N12(2o1)(2o2)-TFSA electrolyte was close to 0.40 V. According to the results of EIS, it could be clearly found that the interfacial resistance of IL electrolyte/lithium metal decreased obviously after cycling test, and it indicated that the passivation layer on lithium metal might change into the SEI film during the C–D processes.

3.4. Charge–discharge characteristics of Li/$LiFePO_4$ cells

The charge–discharge characteristics of Li/$LiFePO_4$ cells using five quaternary ammonium ILs with two ether groups electrolytes and DEME–TFSA electrolyte without additive were examined at room temperature, and the cells were tested under current rate of 0.1 C. Fig. 8 shows the discharge capacity during cycling of Li/$LiFePO_4$ cells using these IL electrolytes. The initial discharge capacity of the cell using DEME–TFSA electrolyte was about 150 mAh g^{-1}, and the discharge capacity decreased gradually with increasing of cycle number. And the discharge capacity retained at about 141 mAh g^{-1} after 50 cycles showing capacity retention of 94%. For the five quaternary ammonium IL with two ether groups electrolytes, N12(2o1)(2o2)-TFSA and N12(2o2)(2o2)-TFSA electrolytes showed higher initial discharge capacity than DEME–TFSA electrolyte at about 152 and 155 mAh g^{-1} respectively, and the

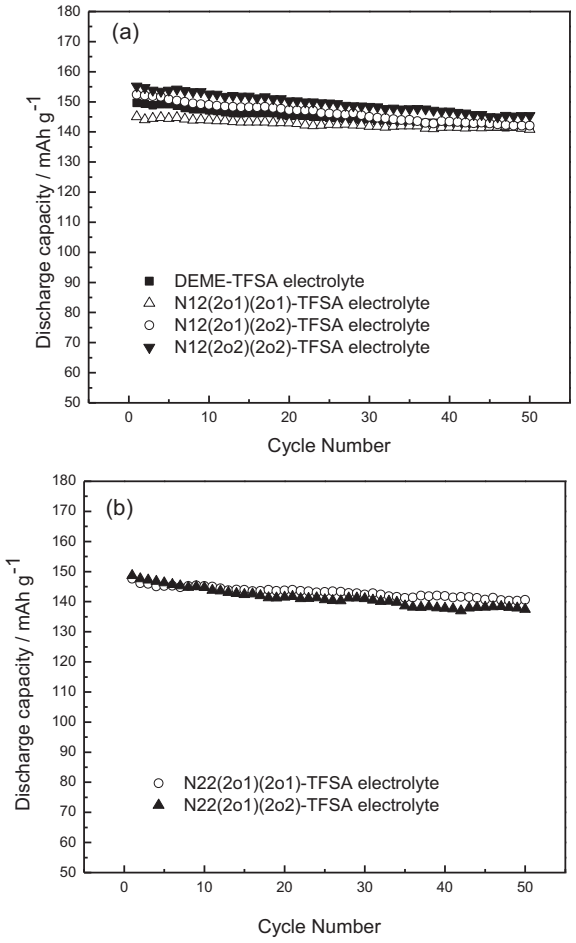

Fig. 8. Cycling performances of Li/$LiFePO_4$ cells using the IL electrolytes with 0.6 mol kg^{-1} LiTFSA at 25 °C, charge–discharge current rate is 0.1 C.

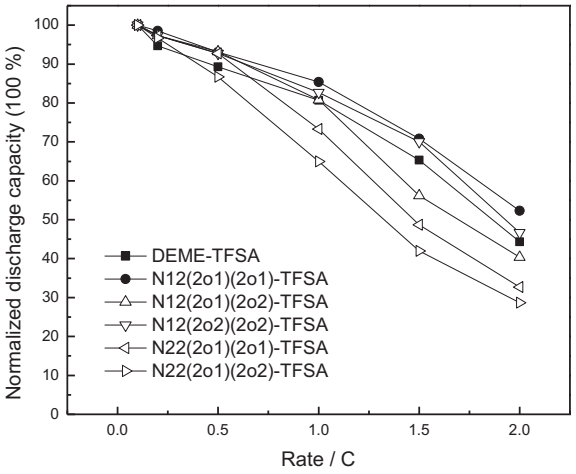

Fig. 9. Rate properties of Li/$LiFePO_4$ cells using the IL electrolytes with 0.6 mol kg^{-1} LiTFSA at 25 °C. Charge current rate is 0.1 C, and discharge current rates are 0.1, 0.2, 0.5, 1.0, 1.5 and 2.0 C.

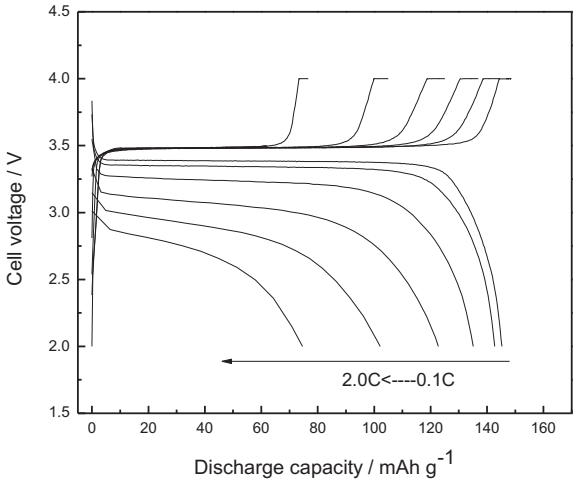

Fig. 10. Charge–discharge curves of Li/$LiFePO_4$ cells using N12(2o1)(2o1)-TFSA electrolyte with 0.6 mol kg^{-1} LiTFSA at different rates at 25 °C. Charge current rate is 0.1 C, and discharge current rates are 0.1, 0.2, 0.5, 1.0, 1.5 and 2.0 C.

initial discharge capacities of N22(2o1)(2o1)-TFSA, N22(2o1)(2o2)-TFSA electrolytes were close to DEME–TFSA electrolyte while N12(2o1)(2o1)-TFSA owned a slightly smaller initial discharge capacity at about 145 mAh g^{-1}. For the capacity retention after 50 cycles aspect, the N12(2o1)(2o1)-TFSA and N22(2o1)(2o1)-TFSA electrolytes had higher capacity retention than DEME–TFSA electrolyte at about 97% and 95%, and the other three quaternary ammonium ILs with two ether groups electrolytes owned capacity retention close to DEME–TFSA electrolyte.

The rate properties of Li/$LiFePO_4$ cells are shown in Fig. 9, during the charge–discharge tests, the cells charge at 0.1 C and discharge at different current rates for 5 cycles, and the discharge capacity is normalized on the basis of discharge capacity at 0.1 C rate. The discharge capacity decreased with increasing of discharge rate. According to Fig. 9, the rate properties of N12(2o1)(2o1)-TFSA and N12(2o2)(2o2)-TFSA electrolytes were better than DEME–TFSA electrolyte, and the rate property of N12(2o1)(2o2)-TFSA electrolyte was close to DEME–TFSA. For instance, as shown in Fig. 10, the discharge capacity for the N12(2o1)(2o1)-TFSA electrolyte at the discharge rate of 1.0 C was about 123 mAh g^{-1}, which retained 85% of the capacity at 0.1 C, and the discharge capacity at the rate of 2.0 C was about 76 mAh g^{-1}, which retained 52% of the capacity at 0.1 C. For the differences of viscosity of these six ILs were not obvious, it was possible that the rate property was affected by some other factors besides the viscosity of IL, such as the interfacial characteristics at both $LiFePO_4$ cathode/electrolyte and lithium metal anode/electrolyte interfaces. And the results of rate performance for these IL electrolytes demonstrated that the introduction of two ether groups in quaternary ammonium cation could also improve the rate performance.

4. Conclusions

Twelve functionalized ILs based on quaternary ammonium cation with two ether groups were synthesized by a facile method. Physical and electrochemical properties, including melting point, thermal stability, viscosity, conductivity and electrochemical window, were investigated for these ILs. All these ILs were liquid at room temperature except N22(2o2)(2o2)-TFSA (T_m = 29.7 °C), and the viscosities of N12(2o1)(2o2)-TFSA and N12(2o2)(2o2)-TFSA were 68.0 cP and 63.0 cP at 25 °C, respectively. Good electrochemical stabilities of these ILs permitted them to become potential electrolytes used in electrochemical devices. Five ILs with lower viscosity were chosen to dissolve 0.6 mol kg^{-1} of LiTFSA as IL electrolytes without additive for lithium battery being compared with DEME–TFSA electrolyte. Behavior of lithium redox on Ni electrode was investigated for these IL electrolytes, and lithium plating and striping on Ni electrode could be observed in these IL electrolytes due to the forming of SEI film. Li/$LiFePO_4$ cells using these quaternary ammonium ILs with two ether groups electrolytes showed good cycle property at 0.1 C current rate, and N12(2o1)(2o1)-TFSA and N12(2o2)(2o2)-TFSA electrolytes owned better rate property than DEME–TFSA electrolyte.

Acknowledgments

The authors thank the Research Center of Analysis and Measurement of Shanghai JiaoTong University for help in NMR characterization. This work was financially supported by the National Natural Science Foundation of China (Grants No. 21103108 and 21173148), the Key Lab of Novel Thin Film Solar Cells, Chinese Academy of Sciences (Grants No. KF201110) and SJTU-UM Research Program (2012).

References

[1] J. Dupont, R.F. de Souza, P.A.Z. Suarez, Chem. Rev. 102 (2002) 3667–3692.
[2] R.D. Rogers, K.R. Seddon, Science 302 (2003) 792–793.
[3] S.A. Forsyth, J.M. Pringle, D.R. MacFarlane, Aust. J. Chem. 57 (2004) 113–119.
[4] M. Armand, F. Endres, D.R. MacFarlane, H. Ohno, B. Scrosati, Nat. Mater. 8 (2009) 621–629.
[5] J.E. Bara, T.K. Carlisle, C.J. Gabriel, D. Camper, A. Finotello, D.L. Gin, R.D. Noble, Ind. Eng. Chem. Res. 48 (2009) 2739–2751.
[6] J. Dupont, J.D. Scholten, Chem. Soc. Rev. 39 (2010) 1780–1804.
[7] J.P. Hallett, T. Welton, Chem. Rev. 111 (2011) 3508–3576.
[8] H. Olivier-Bourbigou, L. Magna, D. Morvan, Appl. Catal. A General 373 (2010) 1–56.
[9] P. Sun, D.W. Armstrong, Anal. Chim. Acta 661 (2010) 1–16.
[10] A. Balducci, S.S. Jeong, G.T. Kim, S. Passerini, M. Winter, M. Schmuck, G.B. Appetecchi, R. Marcilla, D. Mecerreyes, V. Barsukov, V. Khomenko, I. Cantero, I. De Meatza, M. Holzapfel, N. Tran, J. Power Sources 196 (2011) 9719–9730.
[11] V. Borgel, E. Markevich, D. Aurbach, G. Semrau, M. Schmidt, J. Power Sources 189 (2009) 331–336.
[12] M. Chai, Y. Jin, S. Fang, L. Yang, S.-i. Hirano, K. Tachibana, J. Power Sources 216 (2012) 323–329.
[13] M. Egashira, A. Kanetomo, N. Yoshimoto, M. Morita, J. Power Sources 196 (2011) 6419–6424.
[14] S. Fang, Y. Tang, X. Tai, L. Yang, K. Tachibana, K. Kamijima, J. Power Sources 196 (2011) 1433–1441.
[15] A. Lewandowski, A. Świderska-Mocek, J. Power Sources 194 (2009) 601–609.
[16] A.B. McEwen, H.L. Ngo, K. LeCompte, J.L. Goldman, J. Electrochem. Soc. 146 (1999) 1687–1695.
[17] T. Sato, G. Masuda, K. Takagi, Electrochim. Acta 49 (2004) 3603–3611.
[18] A. Orita, K. Kamijima, M. Yoshida, L. Yang, J. Power Sources 195 (2010) 6970–6976.
[19] E. Zygadło-Monikowska, Z. Florjańczyk, P. Kubisa, T. Biedroń, A. Tomaszewska, J. Ostrowska, N. Langwald, J. Power Sources 195 (2010) 6202–6206.
[20] E. Zygadło-Monikowska, Z. Florjańczyk, K. Słuzewska, J. Ostrowska, N. Langwald, A. Tomaszewska, J. Power Sources 195 (2010) 6055–6061.
[21] P. Wang, S.M. Zakeeruddin, M. Grätzel, W. Kantlehner, J. Mezger, E.V. Stoyanov, O. Scherr, Appl. Phys. A Mater. Sci. Process. 79 (2004) 73–77.
[22] D. Kuang, P. Wang, S. Ito, S.M. Zakeeruddin, M. Grätzel, J. Am. Chem. Soc. 128 (2006) 7732–7733.
[23] F. Mazille, Z. Fei, D. Kuang, D. Zhao, S.M. Zakeeruddin, M. Grätzel, P.J. Dyson, Inorg. Chem. 45 (2006) 1585–1590.
[24] S.S. Zhang, Electrochim. Acta 97 (2013) 226–230.
[25] S.Y. Ku, S.Y. Lu, Int. J. Electrochem. Sci. 6 (2011) 5219–5227.
[26] V. Chakrapani, F. Rusli, M.A. Filler, P.A. Kohl, J. Phys. Chem. C 115 (2011) 22048–22053.
[27] M.L.P. Le, F. Alloin, P. Strobel, J.C. Leprêtre, C.P. Del Valle, P. Judeinstein, J. Phys. Chem. B 114 (2010) 894–903.
[28] S.K. Martha, E. Markevich, V. Burgel, G. Salitra, E. Zinigrad, B. Markovsky, H. Sclar, Z. Pramovich, O. Heik, D. Aurbach, I. Exnar, H. Buqa, T. Drezen, G. Semrau, M. Schmidt, D. Kovacheva, N. Saliyski, J. Power Sources 189 (2009) 288–296.
[29] S. Seki, Y. Ohno, H. Miyashiro, Y. Kobayashi, A. Usami, Y. Mita, N. Terada, K. Hayamizu, S. Tsuzuki, M. Watanabe, J. Electrochem. Soc. 155 (2008) A421–A427.

[30] H. Sakaebe, H. Matsumoto, K. Tatsumi, Electrochim. Acta 53 (2007) 1048–1054.
[31] H. Zheng, B. Li, Y. Fu, T. Abe, Z. Ogumi, Electrochim. Acta 52 (2006) 1556–1562.
[32] K. Yuyama, G. Masuda, H. Yoshida, T. Sato, J. Power Sources 162 (2006) 1401–1408.
[33] H. Matsumoto, H. Sakaebe, K. Tatsumi, M. Kikuta, E. Ishiko, M. Kono, J. Power Sources 160 (2006) 1308–1313.
[34] M. Egashira, M. Tanaka-Nakagawa, I. Watanabe, S. Okada, J.i. Yamaki, J. Power Sources 160 (2006) 1387–1390.
[35] H. Zheng, H. Zhang, Y. Fu, T. Abe, Z. Ogumi, J. Phys. Chem. B 109 (2005) 13676–13684.
[36] Y.J. Kim, Y. Matsuzawa, S. Ozaki, K.C. Park, C. Kim, M. Endo, H. Yoshida, G. Masuda, T. Sato, M.S. Dresselhaus, J. Electrochem. Soc. 152 (2005) A710–A715.
[37] M. Egashira, M. Nakagawa, I. Watanabe, S. Okada, J.I. Yamaki, J. Power Sources 146 (2005) 685–688.
[38] H. Sakaebe, H. Matsumoto, Electrochem. Commun. 5 (2003) 594–598.
[39] H. Sakaebe, H. Matsumoto, K. Tatsumi, J. Power Sources 146 (2005) 693–697.
[40] J.H. Davis Jr., Chem. Lett. 33 (2004) 1072–1077.
[41] Z. Fei, T.J. Geldbach, D. Zhao, P.J. Dyson, Chem.—Eur. J. 12 (2006) 2122–2130.
[42] S. Seki, Y. Kobayashi, H. Miyashiro, Y. Ohno, Y. Mita, A. Usami, N. Terada, M. Watanabe, Electrochem. Solid-State Lett. 8 (2005) A577–A578.
[43] K. Tsunashima, F. Yonekawa, M. Sugiya, Electrochem. Solid-State Lett. 12 (2009) A54.
[44] T. Sato, T. Maruo, S. Marukane, K. Takagi, J. Power Sources 138 (2004) 253–261.
[45] A. Lewandowski, A. Swiderska-Mocek, L. Waliszewski, M. Galinski, J. Power Sources 197 (2012) 292–296.
[46] A. Lewandowski, I. Acznik, A. Swiderska-Mocek, J. Appl. Electrochem. 40 (2010) 1619–1624.
[47] S. Ferrari, E. Quartarone, P. Mustarelli, A. Magistris, S. Protti, S. Lazzaroni, M. Fagnoni, A. Albini, J. Power Sources 194 (2009) 45–50.
[48] M.J. Monteiro, F.F. Camilo, M.C.C. Ribeiro, R.M. Torresi, J. Phys. Chem. B 114 (2010) 12488–12494.
[49] J. Jin, H.H. Li, J.P. Wei, X.K. Bian, Z. Zhou, J. Yan, Electrochem. Commun. 11 (2009) 1500–1503.
[50] M. Kärnä, M. Lahtinen, J. Valkonen, J. Mol. Struct. 922 (2009) 64–76.
[51] H.B. Han, K. Liu, S.W. Feng, S.S. Zhou, W.F. Feng, J. Nie, H. Li, X.J. Huang, H. Matsumoto, M. Armand, Z.B. Zhou, Electrochim. Acta 55 (2010) 7134–7144.
[52] S. Fang, Y. Jin, L. Yang, S.I. Hirano, K. Tachibana, S. Katayama, Electrochim. Acta 56 (2011) 4663–4671.
[53] K. Tsunashima, M. Sugiya, Electrochemistry 75 (2007) 734–736.
[54] Z.-B. Zhou, H. Matsumoto, K. Tatsumi, Chem.—Eur. J. 12 (2006) 2196–2212.
[55] Z.-B. Zhou, H. Matsumoto, K. Tatsumi, Chem.—Eur. J. 11 (2005) 752–766.
[56] Z.-B. Zhou, H. Matsumoto, K. Tatsumi, Chem.—Eur. J. 10 (2004) 6581–6591.
[57] S. Fang, L. Yang, J. Wang, M. Li, K. Tachibana, K. Kamijima, Electrochim. Acta 54 (2009) 4269–4273.
[58] Y. Jin, S. Fang, L. Yang, S.-i. Hirano, K. Tachibana, J. Power Sources 196 (2011) 10658–10666.
[59] Y. Jin, S. Fang, M. Chai, L. Yang, S.-i. Hirano, Ind. Eng. Chem. Res. 51 (2012) 11011–11020.
[60] S. Fang, Z. Zhang, Y. Jin, L. Yang, S.-i. Hirano, K. Tachibana, S. Katayama, J. Power Sources 196 (2011) 5637–5644.
[61] S. Fang, L. Yang, J. Wang, H. Zhang, K. Tachibana, K. Kamijima, J. Power Sources 191 (2009) 619–622.
[62] P. Bonhôte, A.-P. Dias, M. Armand, N. Papageorgiou, K. Kalyanasundaram, M. Grätzel, Inorg. Chem. 37 (1998), 166–166.
[63] Z.J. Chen, T. Xue, J.-M. Lee, RSC Adv. 2 (2012) 10564–10574.
[64] N.A. Stolwijk, S. Obeidi, Electrochim. Acta 54 (2009) 1645–1653.
[65] R. Sescousse, K.A. Le, M.E. Ries, T. Budtova, J. Phys. Chem. B 114 (2010) 7222–7228.
[66] J. Sun, M. Forsyth, D.R. MacFarlane, J. Phys. Chem. B 102 (1998) 8858–8864.
[67] J. Xu, J. Yang, Y. NuLi, J. Wang, Z. Zhang, J. Power Sources 160 (2006) 621–626.
[68] H. Matsumoto, H. Sakaebe, K. Tatsumi, J. Power Sources 146 (2005) 45–50.
[69] A.S. Best, A.I. Bhatt, A.F. Hollenkamp, J. Electrochem. Soc. 157 (2010) A903–A911.
[70] A.I. Bhatt, A.S. Best, J. Huang, A.F. Hollenkamp, J. Electrochem. Soc. 157 (2010) A66–A74.
[71] G.H. Lane, A.S. Best, D.R. MacFarlane, A.F. Hollenkamp, M. Forsyth, J. Electrochem. Soc. 157 (2010) A876–A884.
[72] H. Yoon, G.H. Lane, Y. Shekibi, P.C. Howlett, M. Forsyth, A.S. Best, D.R. MacFarlane, Energy Environ. Sci. 6 (2013) 979–986.
[73] Y. Jin, S. Fang, M. Chai, L. Yang, S.-i. Hirano, Ind. Eng. Chem. Res. 51 (2012) 11011–11020.
[74] A. Fernicola, F. Croce, B. Scrosati, T. Watanabe, H. Ohno, J. Power Sources 174 (2007) 342–348.
[75] S. Seki, Y. Ohno, Y. Kobayashi, H. Miyashiro, A. Usami, Y. Mita, H. Tokuda, M. Watanabe, K. Hayamizu, S. Tsuzuki, M. Hattori, N. Terada, J. Electrochem. Soc. 154 (2007) A173–A177.
[76] A.I. Bhatt, A.S.B.P. Kao, A.F. Hollenkamp, ECS Trans. 50 (2012) 383–401.